C-arm flat-panel CT arthrography of the wrist and elbow: first experiences in human cadavers

**Roman Guggenberger · Fabian Morsbach ·
Hatem Alkadhi · Magdalena Vich ·
Thomas Pfammatter · Juerg Hodler · Gustav Andreisek**

Abstract

Objective To determine the optimal intra-articular iodine concentration for C-arm flat-panel computed tomography (FPCT) arthrography using advanced joint phantoms and to evaluate its application in human cadaveric wrists and elbows. Multi-detector (MD) CT served as the standard of reference.

Materials and methods Joint phantoms and 10 human cadaveric wrist and elbow joints were scanned with C-arm FPCT (5-s, 8-s, and 20-s runs) and standard MDCT using different and optimal concentrations of iodinated contrast material. CT numbers of contrast material, tissue, and noise were measured and contrast-to-noise ratios (CNR) calculated for quantitative analysis. Image and depiction of cartilage, bone, and soft tissues were rated. Radiation doses were compared.

Results In FPCT, iodine concentrations positively correlated with CT numbers and noise of contrast material and with radiation dose ($r=0.713$–0.996, $p<0.05$ each). At an iodine concentration of 45 mg/ml, CNR of cartilage and soft tissues were highest for all FPCT acquisitions and higher than in MDCT. The 20-s FPCT run performed best for image quality and depiction of anatomical structures and was rated overall equal to MDCT ($p=0.857$).

Conclusion The optimal iodine concentration for C-arm FPCT arthrography in this study is 45 mg/ml, leading to superior CNR and image quality for an optimal FPCT protocol compared with standard MDCT arthrography in human cadaveric joints.

R. Guggenberger (✉) · F. Morsbach · H. Alkadhi ·
T. Pfammatter · J. Hodler · G. Andreisek
Department of Radiology, University Hospital Zurich,
Ramistrasse 100,
8091 Zurich, Switzerland
e-mail: roman.guggenberger@usz.ch

M. Vich
Institute of Anatomy, University Zurich,
Winterthurerstrasse 190,
8057 Zurich, Switzerland

Introduction

Evaluation of different joint components with emphasis on cartilage is essential in the detection and quantification of joint pathology but relies upon high spatial resolution of the applied imaging procedure [1]. Multidetector computed tomography (MDCT) is routinely performed for direct CT arthrography of joints using intra-articular injection of iodinated contrast material [2–4]. It is appreciated by clinicians and radiologists alike due to its wide availability and excellent quality in detection of bone and cartilage surface defects with often superior spatial resolution compared to magnetic resonance (MR) imaging [5, 6].

Spatial resolution of MDCT is limited by current detector designs which typically allow a maximal z-resolution of 0.4–0.5 mm [7]. This is usually enough to detect most cartilage lesions in CT arthrography [2, 3, 8]. Flat-panel (FP) detectors which consist of cesium-iodide (CsI) scintillator crystals however differ in physical design and potentially enable much higher spatial resolution with isotropic voxel sizes of up to 0.154 mm [9, 10]. New cone beam CTs use FP detectors and have recently been shown to allow for accurate wrist assessment at high spatial resolution [11] including the intrinsic wrist ligaments when CT arthrography is performed [12]. Modern angiographic systems are also typically equipped with these FP detectors. Mounted on a flexible C-arm, these systems provide projections from different angulations at predefined rotation angles. Since the acquired raw data are

three-dimensional and secondary multi-planar reconstructions with high isotropic resolution are possible, this technique is usually referred to as C-arm flat-panel computed tomography (FPCT) analogous to MDCT.

Although detectors of MDCT scanners offer substantial z-coverage, X-ray beam geometry in MDCT is conceptually considered as fan beam versus cone beam geometry in FPCT [13]. Rotational tomography in the C-arm FPCT is usually performed in a 200° rotation of the gantry versus 360° rotation in MDCT [14, 15]. FPCT typically operates at a lower tube voltage than MDCT (70 kV versus 100–140 kV, respectively). All those technical differences may influence image noise, contrast of biologic tissues and optimal iodine concentrations [16] and hamper straightforward comparisons of FPCT and MDCT in research and 1:1 use in clinical practice.

In the past, FPCT has been successfully used for various interventional procedures in the abdomen, head or spine [17–20], and for the evaluation of trabecular bone microstructure [21–23]. Recently, a study has shown the feasibility C-arm FPCT arthrography using a quite simple phantom and animal cadaver model [24]. Although this study was proof of principle, first results on this new technique were encouraging as the image quality in this early trial was already comparable to standard MDCT, at least when optimal iodine concentrations and imaging parameters were used [24]. However, it is not clear if imaging parameters and iodine concentration may be applicable to human anatomy as well. We hypothesized that the optimal iodine concentration for C-arm FPCT arthrography is likely to be different i.e. with regard to the optimal depiction of anatomical structures such as cartilage and bone.

Thus, the purpose of our study was to determine the optimal intra-articular iodine concentration for C-arm FPCT arthrography using advanced biologic joint phantoms and to evaluate its application in humans using cadaver wrists and elbows. MDCT served as standard of reference.

Materials and methods

According to local regulations and laws, cantonal ethics board approval was not required for this prospective human cadaver study. Institutional review board approved this study, which was conducted according to the Declaration of Helsinki. All cadaveric specimens were treated in accordance with the University's and institution's regulations on cadaveric studies.

Advanced joint phantoms

Spherical joint phantoms were constructed in order to test for the optimal concentration of intra-articular iodinated contrast material for FPCT arthrography. Therefore, plastic spheres with a diameter of 8 cm and a thickness of 1.5 mm were cut into two identical hemispheres at the equator. Tibial epiphyses with soft tissue remnants (connective and muscle tissue) of cadaveric pig knees were mounted on each side of a circular plastic plane (2 mm in thickness), which was then fixed in the center of the spheres. Both hemispheres were sealed together using a water-proof tape and eventually filled with increasing concentrations of iodine (0, 15, 45, 100, and 150 mg iodine/ml) via a small drill hole of 2 mm in diameter. Iodine concentrations were attained by decreasing dilutions of iopromide (Ultravist 300 mg iodine/ml, Bayer HealthCare, Berlin, Germany) with saline. The joint phantoms were placed in the center of the FPCT and MDCT unit, aligned with their longitudinal axis to the z-axis of the scanner tables (Fig. 1).

Human cadaveric joints

Five human wrists and human elbows from 3 different subjects (2 men, 1 woman; age at death not known) were available for the human cadaveric experiments. Based on the results from the advanced joint phantom experiments, the iodine concentration, which provided the optimal contrast-to-noise ratio (CNR) for various biological tissues (see Results section below) was chosen (45 mg iodine/ml) and injected under fluoroscopic guidance.

Wrists were injected dorsally using a two-compartmental approach with two separate injections at the distal radio-ulnar joint and at the four-angle corner of the carpus (i.e., among the hamate, capitate, lunate, and triquetrum) respectively [25]. Elbow joints were injected using a lateral approach where the contrast material was injected between the radial head and the humeral capitulum [26].

On average, 2–4 ml of contrast material was injected into the wrist joint and 5–7 ml into the elbow joint. Fluoroscopy-guided contrast material injection into all 10 joints was performed in the same C-arm FPCT unit as used for subsequent rotational tomography. MDCT arthrography was immediately performed after FPCT arthrography with a maximum delay of 5±3 min between the two examinations.

Flat-panel CT acquisitions

Flat-panel CT acquisitions were performed on an angiographic unit (Artis Zeego multi-axis system, Siemens Healthcare, Forchheim, Germany) with a C-arm-mounted FP detector. The FP detector (30×38 cm) was operated in a standard 2×2 binning mode where four neighboring detector pixels, each of 154 μm size, are read out together to allow an increase in the number of frames that can be read out per second.

Similar to the recent feasibility study of Guggenberger et al. [24], three different imaging protocols for FPCT were

Fig. 1 Axial images of advanced joint phantoms tibial epiphyses of cadaveric pig knees mounted in a bi-hemispheric plastic model filled with iodinated contrast agent (in this example, at an iodine concentration of 45 mg/ml). Joint phantoms were scanned in flat panel CT (FPCT; **a**, 5-s,**b** 8-s, and **c** 20-s runs) and **d** multidetector (MDCT). Note increasing image quality and depictability of anatomical structures with decreasing image noise from the 5-s to the 20-s FPCT run (**a**–**c**). Also, note the similar noise levels of the FPCT 5-s run (**a**) and MDCT (**d**)
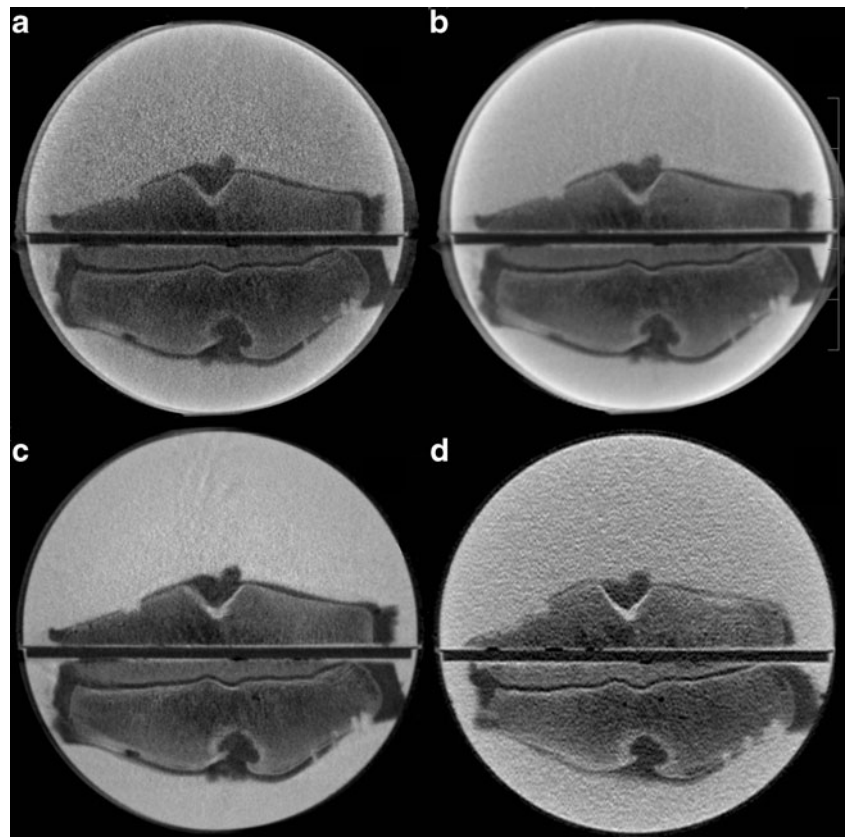
used. Protocols mainly differed in total scan duration: 5, 8 and 20 s, respectively. For the 5-s and the 20-s runs vendor-specific default pre-settings were used. They were originally designed by the vendor for abdominal and neuro-vascular interventional applications respectively. The 8-s run, however, was custom-made to imitate the intermediate protocol used in the aforementioned feasibility study [24]. This intermediate protocol was originally designed as a trade-off between the 5-s and the 20-s run with respect to scan duration and radiation dose.

The 5-s, 8-s, and 20-s runs had different angulation steps (1.5°, 0.5° and 0.4° respectively), which resulted in three different numbers of projections (133, 400, and 500 respectively) as well as different scan durations for the standard 200° rotation of the C-arm around the object. Other scan parameters were: tube voltage, 70 kV; distance from the source to the axis of rotation, 78.5 cm; distance from the source to the image plane, 120 cm. Collimation of the field-of-view of FPCT was kept constant for all scans. The angiography unit automatically calculated the tube current–time product as well as the dose–area product (DAP in μGym^2), which are parameters for the radiation dose.

Multidetector CT acquisitions

A 64-section CT unit (Definition AS, Siemens Healthcare, Forchheim, Germany) was used for MDCT employing the standard clinical protocol, which is usually used for CT arthrography of the wrist and elbow at our department. The protocols include use of automated attenuation-based tube–current modulation (CAREDose4D, Siemens) and the z-flying focal spot technique. The detector collimation was 16×0.3 mm. Other scan parameters were: tube voltage, 120 kV; tube current–time product per rotation, 120 mAs; pitch, 0.85. After each study, the scanner generates automatically a "patient" protocol from which the computed tomography dose index (CTDI$_{vol}$ in mGy) and the dose–length product (DLP in mGy.cm) were recorded as parameters for the radiation dose.

Postprocessing

All image data were transferred to a separate workstation (Leonardo, Siemens). One author (R.G.) used dedicated software (InSpace3D, Siemens) and performed all postprocessing in two steps.

First, axial images of advanced joint phantoms were produced. Therefore, FPCT images were postprocessed by reconstructing axial thin-slice images with a 10-cm volume-of-interest employing a high frequency/bone kernel. Matrix size of reconstructed images was $512 \times 512 \times 512$. This resulted in isotropic voxels of 0.29-mm edge length. MDCT images were also postprocessed by reconstructing axial images at 10-cm field-of-view and 512×512 matrix size. Slice thickness was 0.75 mm, and the increment was 0.4 mm.

For human cadaveric joints, multiplanar reformations (MPR) were calculated from raw data in coronal, sagittal, and axial planes for both FPCT and MDCT. Slice thickness and increment were identical (1 mm and 0.6 mm respectively; Figs. 2, 3).

Axial thin-slice and MPR images were then transferred to the picture archiving and communication system (PACS; IMPAX 6, Agfa-Gaevert N.V., Belgium) for quantitative and qualitative analyses.

Quantitative data analysis

One radiologist (R.G., 2 years of experience in musculoskeletal imaging) blinded to iodine concentration, modality and scan protocols performed quantitative analysis which based on regions-of-interest (ROIs) measurements. ROIs were placed in bone, cartilage and soft tissue as well as in the contrast material filled compartments in both, the phantoms and the human cadavers. Care was taken to place all ROIs on corresponding slices of the FPCT and MDCT images. Within each ROI, attenuation (in Hounsfield units; HU) and noise (standard deviation; SD) were measured. CNRs were then calculated for each anatomical structure as well as for the different acquisition protocols and iodine concentrations. For the latter, the difference in contrast material and tissue attenuation was divided by the contrast material noise.

Qualitative data analysis

First, two independent readers (R.G. and H.A., with 4 and 5 years of experience in musculoskeletal imaging) evaluated all FPCT and MDCT images with regard to three different image parameters: artifacts, noise, and interpretability. A four-point classification system was used for each parameter (4 = diagnostic images without relevant artifacts/noise; excellent interpretability; 3 = diagnostic images with minor artifacts/noise; good interpretability; 2 = diagnostic images, but substantial artifacts/noise; poor interpretability; 1 = nondiagnostic images due to either strong artifacts or noise; not interpretable) [24]. An overall mean image quality score was calculated from these three parameters. Both readers were blinded to iodine concentration, modality, and scan protocols.

Second, to directly compare how well anatomical structures of cartilage, bone and soft tissue are depicted on the individual image modalities, a four-box display layout of the PACS software was chosen by a study assistant (F.M.) to display corresponding images from the three FPCT runs along with the reference MDCT images on a single screen. During this second step, readers were unblinded to modality as they were asked by the study assistant to rate the depictability of the different anatomical structures using a three-point rating scale in comparison to the MDCT images (1=worse, 2=equal or 3=better depictability on FPCT images compared with MDCT). Both readers were, however, still blinded to iodine concentration and scan protocol. Readers were able to choose image zoom factors and window level arbitrarily at their discretion. Finally, the average of the individual ratings of the different anatomical structures was calculated, which would allow overall comparison of the depictability of anatomical structures between FPCT and MDCT.

Fig. 2 Coronal reformations of human cadaveric wrist arthrographies acquired with intra-articular contrast material at an iodine concentration of 45 mg/ml with FPCT **a** 5-s, **b** 8 s, **c** 20-s runs and **d** MDCT. Note increasing overall image quality and decreasing image noise for FPCT from 5 s to 20 s (**a**–**c**). The FPCT 20-s run showed comparable image quality and better depictability of anatomical structures compared with standard MDCT (**d**)
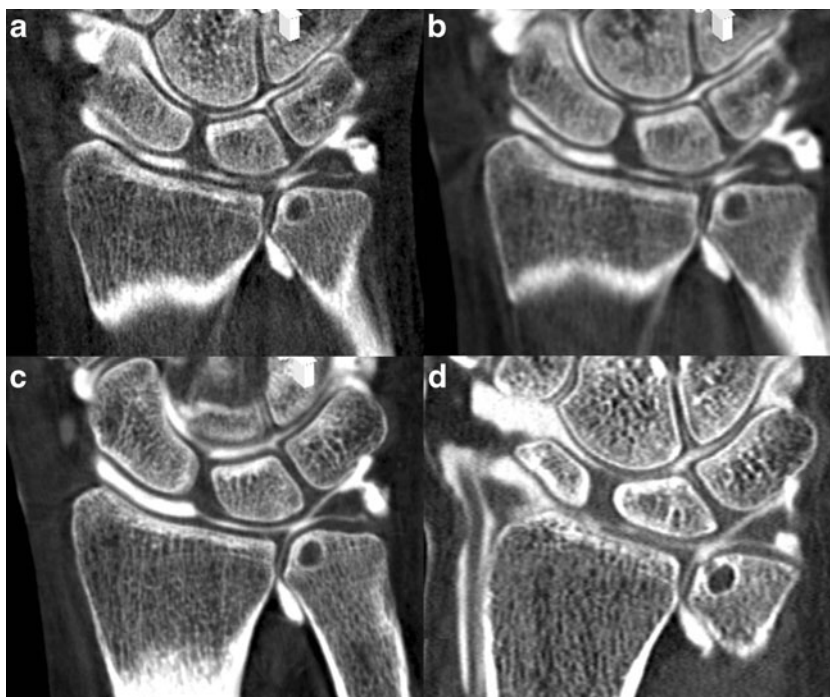
Fig. 3 Coronal reformations of human cadaveric elbow arthrographies acquired with intra-articular contrast material at an iodine concentration of 45 mg/ml with FPCT **a** 5-s, **b** 8-s, **c** 20-s runs and **d** MDCT. Note increasing overall image quality and decreasing image noise for FPCT from the 5-s to the 20-s run (**a**–**c**). The FPCT 20-s run showed comparable image quality and better depictability of anatomical structures compared with standard MDCT (**d**)
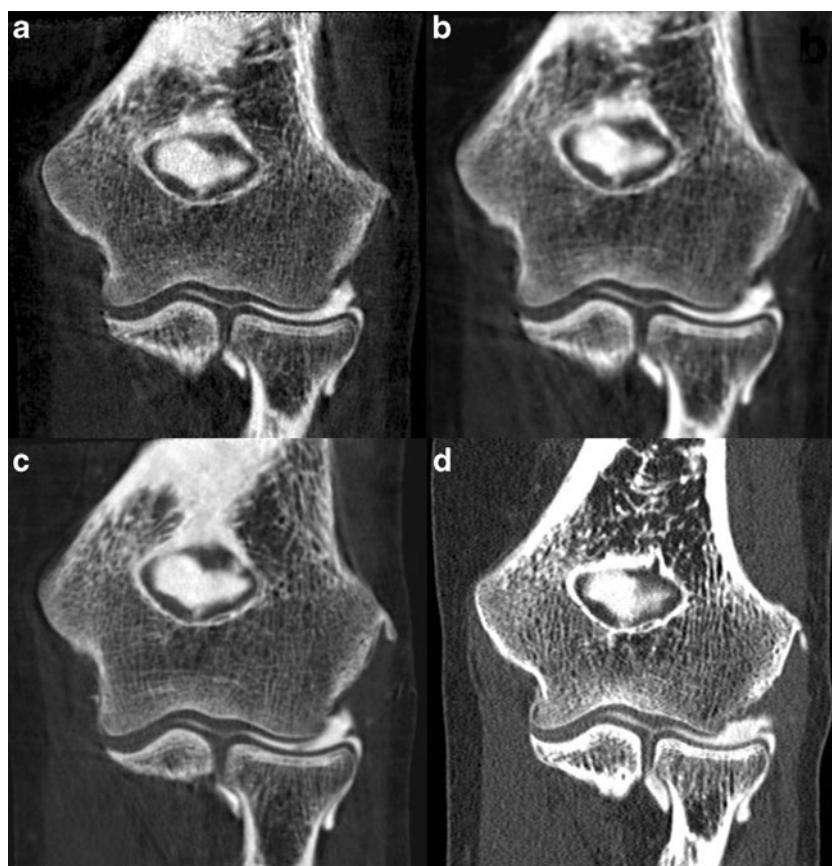
Statistical analysis

All calculations were performed using SPSS software (IBM SPSS Statistics, version 19, IBM, Somers, NY, USA). Descriptive statistics were used to present quantitative data from attenuation, noise, and radiation dose.

In the advanced joint phantoms, bar charts were drawn to illustrate the different CNR values derived from quantitative analyses as well as the rating scores derived from qualitative analyses. Pearson correlation coefficients (r) were calculated to evaluate the association of the increased contrast attenuation and the radiation dose in the different CT acquisitions.

In human cadaveric joints, the related samples Friedman two-way analysis was performed to test for equal distributions and the Wilcoxon signed-rank test was used to test for paired differences of median CNR values between CT acquisitions as well as to compare qualitative median rating scores of different CT acquisitions. Bonferroni corrections for multiple comparisons were applied. Bar charts were drawn to show mean CNR values and mean rating scores for different CT acquisitions.

Kappa values were calculated to assess the inter-reader agreement for qualitative rating scores [27]. According to Landis and Koch, kappa values of 0.61–0.80 were interpreted as substantial, and 0.81–1 as high agreement [28]. A p value of 0.05 was considered statistically significant.

Results

Advanced joint phantoms

Quantitative data analyses

The CNR values of cartilage and soft tissue peaked at an iodine concentration of 45 mg/ml in all FPCT acquisitions. CNR steadily increased for MDCT with increasing iodine concentrations (Fig. 4a, c). The highest CNR for bone was seen for the 8-s and 20-s FPCT runs in the absence of iodine (Fig. 4b).

A strong positive correlation was found between the attenuation (HU values) as well as noise (standard deviation of HU values) of intra-articular contrast material and iodine concentrations ($r = 0.856$–0.992 and 0.713–0.899, all $p < 0.05$; Table 1) in both modalities. Radiation exposure of joint phantoms increased significantly with increasing iodine concentrations for all FPCT acquisitions ($r = 0.996$, 0.992, and 0.995 for the 5-s, 8-s and 20-s runs respectively; $p < 0.001$) while remaining constant for MDCT ($p = 0.55$).

Qualitative data analyses

Kappa values for the evaluation of artifacts, noise, and image interpretability as well as for the rating of depictability of the
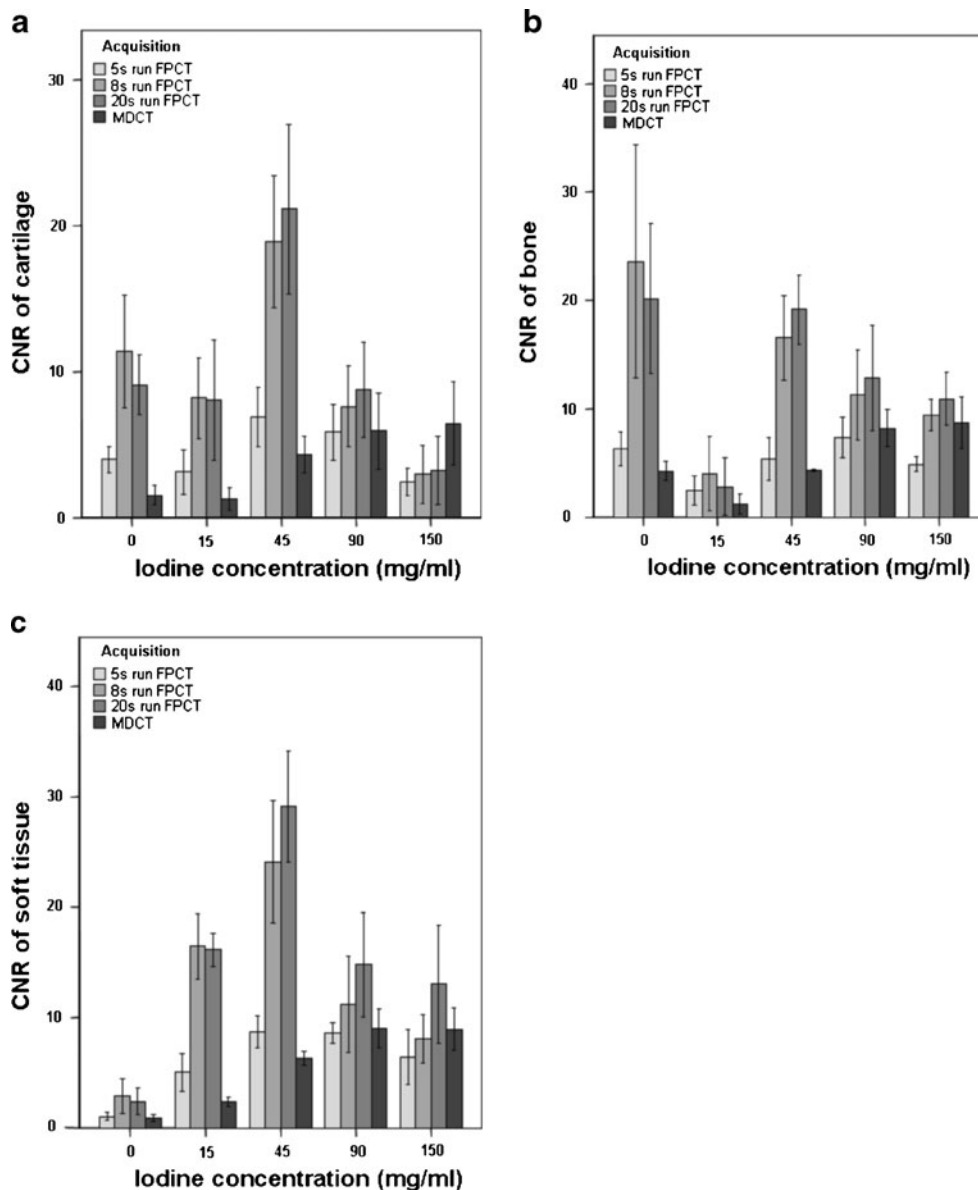
Fig. 4 Contrast-to-noise ratios (CNR) of the three different tissue types, **a** cartilage, **b** bone, and **c** soft tissue with increasing iodine concentrations of contrast material in advanced joint phantoms. Note: the maximal CNR of cartilage and soft tissue was found at an iodine concentration of 45 mg/ml for all FPCT acquisitions (**a**, **c**). CNR of bone was highest in the absence of iodine (**b**). In contrast to FPCT acquisitions, CNR in MDCT steadily increased with increasing iodine concentrations of contrast material for all tissue types (**a–c**)

different anatomical structures (bone, cartilage, and soft tissue) were 0.699–0.846 ($p<0.05$) and 0.767–0.957 ($p<0.001$) respectively. According to Landis and Koch's interpretation, this corresponds to a substantial to high inter-reader agreement [28].

The best overall image quality was seen at an iodine concentration of 45 mg/ml for all FPCT acquisitions. At that concentration, image quality of the 20-s run was better than any of the other MDCT scans (Fig. 5a). For the latter, data revealed that image quality remains almost the same regardless of the iodine concentration used. With MDCT as the standard of reference, the best depictability of anatomical

structures (cartilage, bone, soft tissues) on FPCT arthrographies was found at iodine concentrations of 45 mg/ml. This was true for all three FPCT acquisitions, the 5-s, 8-s and the 20-s runs (Fig. 5b).

Human cadaveric joints

Quantitative data analyses

Radiation dose of the different wrist and elbow FPCT arthrographies increased with increasing scan duration. The lowest radiation dose was seen for the fastest FPCT run (5 s; Table 2).

Table 1 Mean attenuation (CT numbers) and noise (standard deviation of CT numbers) of contrast material in advanced joint phantoms

Iodine concentration (mg/ml)	5-s run FPCT		8-s run FPCT		20-s run FPCT		MDCT	
	Mean HU (± SD)	Mean noise (± SD)	Mean HU (±SD)	Mean noise (± SD)	Mean HU (±SD)	Mean noise (± SD)	Mean HU (±SD)	Mean noise (± SD)
0	17.2 (±17.0)	108.2 (±30.6)	53.4 (±15.2)	30.3 (±6.4)	36.3 (±18.6)	111.5 (±38.9)	2.8 (±2.5)	89.8 (±11.1)
15	658.3 (±131.7)	93.8 (±8.6)	732.6 (±125.7)	32.0 (±4.1)	683.6 (±110.8)	37.7 (±7.5)	316.9 (±53.3)	91.6 (±8.6)
45	1695.8 (±163.5)	139.9 (±8.8)	1805.8 (±107.1)	55.7 (±16.1)	1666.7 (±128.5)	33.4 (±3.7)	874.4 (±12.8)	117.1 (±13.3)
90	2296 (±218.7)	169.9 (±8.6)	2523 (±213.0)	165.5 (±88.9)	2102.3 (±287.6)	44.4 (±7.3)	1580.8 (±78.9)	155.7 (±27.8)
150	2325.5 (±266.3)	158.1 (±35.8)	2316.8 (±89.6)	111.5 (±38.9)	2149.8 (±180.7)	101.8 (±35.4)	2208.3 (±41.0)	219.6 (±46.1)

Attenuation increased with increasing iodine concentration in FPCT acquisitions (5-s, 8-s, and 20-s run) and MDCT

FPCT flat-panel computed tomography, *MDCT* multi-detector computed tomography, ± *SD* ± standard deviation

Measured CNR values of the 5-s run were, however, lowest among all three FPCT runs (Fig. 6). The highest CNR for all three tissue types (cartilage, bone, and soft tissue) was seen in the 20-s FPCT runs, followed by the 8-s FPCT runs. CNR of standard MDCT was found to be similar to the 5-s run and, therefore, lower as in the 8-s and 20-s FPCT runs. There was no statistically significant difference in CNR between the 5-s runs and MDCTs. Differences in CNR among FPCT and MDCT acquisitions were significant ($p<0.001$) as well as the paired differences of CNR between the 20-s and 5-s FPCT runs, 20-s FPCT runs and MDCT as well as 8-s FPCT runs and MDCT (all $p<0.01$; Fig. 6).

Qualitative data analyses

Kappa values for image artifacts, noise, and image interpretability, as well as for rating the depictability of the different anatomical structures (bone, cartilage, and soft tissue) were 0.649–0.750 ($p<0.01$) and 0.657–0.93 ($p<$ 0.05) respectively. According to Landis and Koch's interpretation, this corresponds to a substantial to high inter-reader agreement [28]. The best overall image quality was seen in the 20-s FPCT runs. Image quality of the 20-s runs did not differ from MDCT ($p=0.857$). Both, the 20-s FPCT run and MDCT thus showed superior image quality compared with the 5-s and 8-s FPCT runs (all $p<0.01$). Image quality of the FPCT wrist arthrographies was always slightly better than that of the elbow arthrographies. Vice versa in MDCT where elbow arthrographies had a slightly better image quality compared with the wrist arthrographies. However, all those joint-to-joint differences were not statistically significant ($p>0.05$; Fig. 7a).

With MDCT as the standard of reference, the 20-s FPCT runs provided the best depictability of anatomical structures (cartilage, bone, soft tissues). Differences compared with the inferior 5-s and 8-s FPCT runs were statistically significant ($p<0.01$; Fig. 7b).

Fig. 5 **a** Mean ratings of overall image quality of advanced joint phantoms show highest ratings for contrast material at an iodine concentration of 45 mg/dl in FPCT acquisitions, while ratings in MDCT remained comparably high at different iodine concentrations. **b** Mean ratings of depictability of anatomical structures in FPCT acquisitions in relation to MDCT were best at an iodine concentration of 45 mg/dl
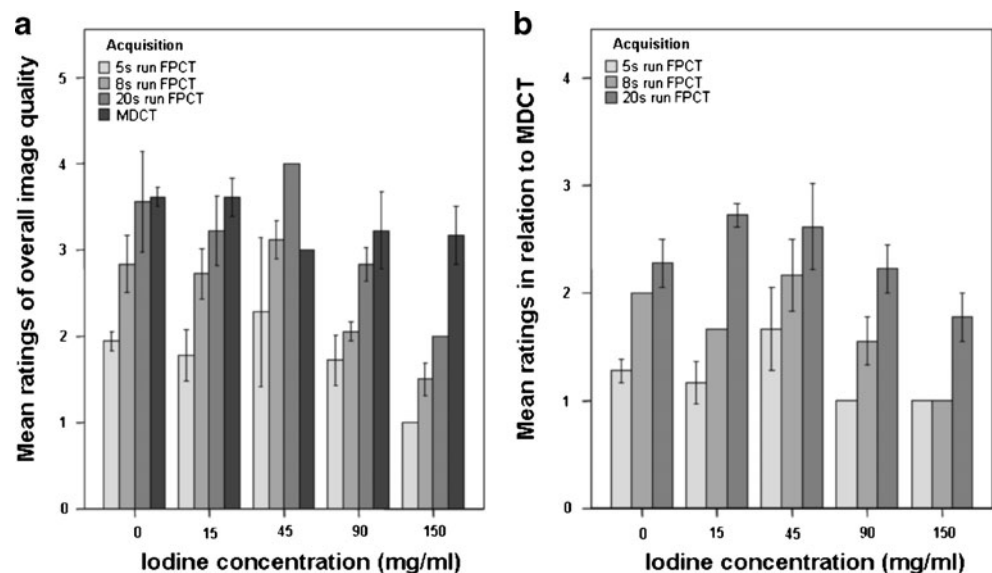
Table 2 Mean radiation dose of FPCT acquisitions (5-s, 8-s and 20-s run) and MDCT in human cadaveric joint arthrographies

Joint	5-s FPCT run (μGym^2) Mean ($\pm$ SD)	8-s FPCT run (μGym^2) Mean ($\pm$SD)	20-s FPCT run (μGym^2) Mean ($\pm$SD)	MDCT (mGy.cm) Mean ($\pm$SD)
Wrist	40.6 ($\pm$12.9)	113.8 ($\pm$35.7)	442.0 ($\pm$136.9)	137.3 ($\pm$18.9)
Elbow	72.8 ($\pm$9.7)	249.9 ($\pm$84.1)	816 ($\pm$145.4)	143.3 ($\pm$14.8)

Radiation dose for FPCT is given as a dose–area product in μGym^2 and as dose–length product in mGy.cm for MDCT. Cadaveric joints were injected with contrast material at an iodine concentration of 45 mg/ml

FPCT flat panel computed tomography, *MDCT* multidetector computed tomography, $\pm$ *SD* $\pm$ standard deviation

Discussion

To the best of our knowledge, our ex vivo study describes the first experience of using a flexible C-arm flat-panel system for FPCT arthrography of human joints. Results demonstrate that C-arm FPCT arthrography of the human wrist and elbow joint, when optimally performed at an intra-articular iodine concentration of 45 mg/ml, provides at least

Fig. 6 Contrast-to-noise ratios (CNR) of the three different tissue types, **a** cartilage, **b** bone, and **c** soft tissue in human cadaveric wrist and elbow joint arthrographies calculated for different CT acquisitions and performed at an iodine concentration of 45 mg/ml of the intra-articular contrast material. Note that CNR in all FPCT acquisitions was equal to or higher than in MDCT owing to lower tube voltage (70 kV in FP vs 120 kV in MDCT) and consecutively higher CT numbers of contrast material (**a–c**). The maximal CNR of all tissue types was reached in 20-s FPCT runs owing to minimal noise
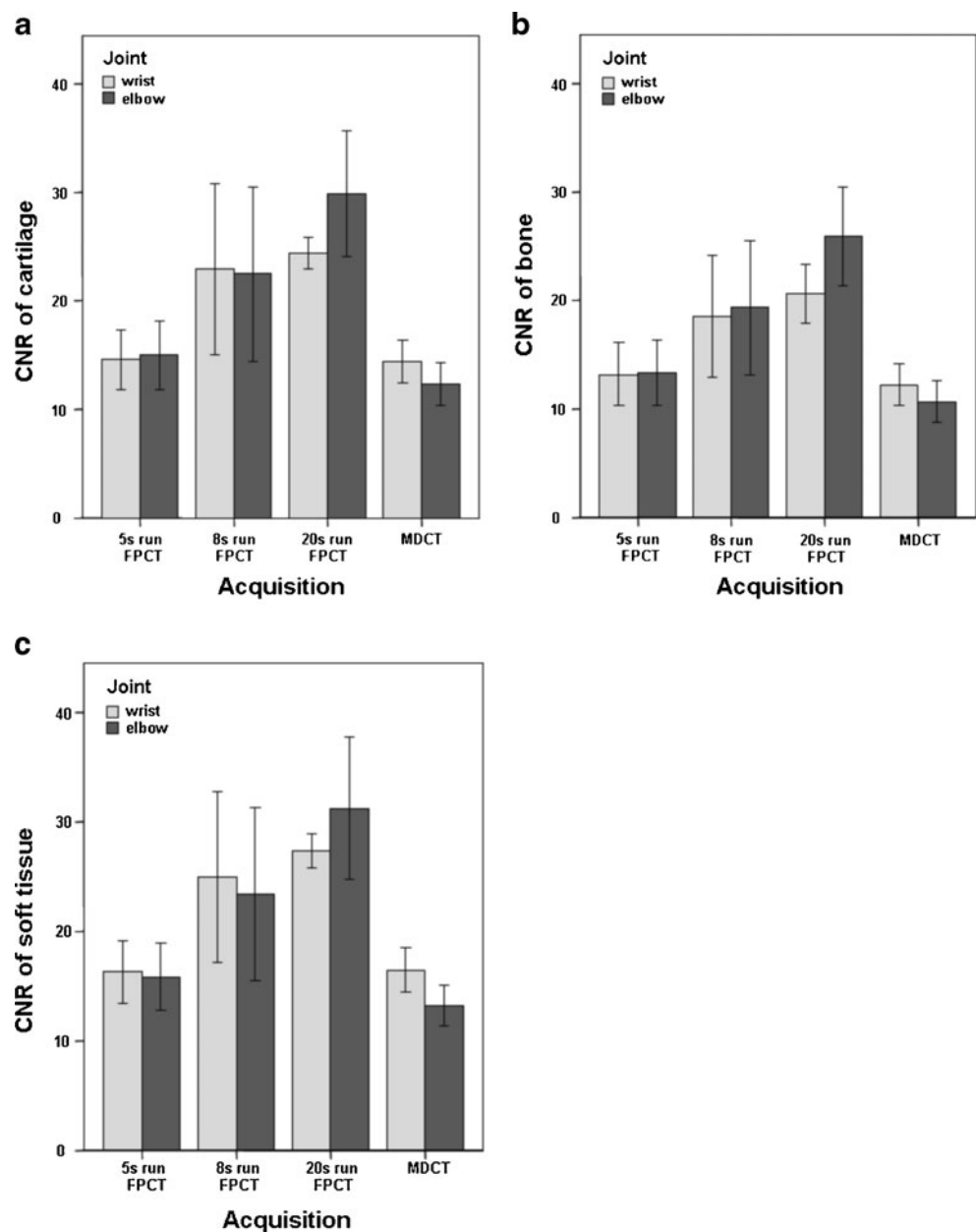
Fig. 7 a Mean ratings of overall image quality of human cadaveric wrist and elbow CT arthrographies at an iodine concentration of the intra-articular contrast material of 45 mg/dl show comparable ratings for 20-s FPCT runs and MDCT. **b** Mean ratings of different FPCT acquisitions in relation to MDCT showed better depiction of tissues for the 20-s FPCT run. 5-s FPCT runs were rated worse, while 8-s FPCT runs showed nearly equal depiction quality of tissues compared with MDCT
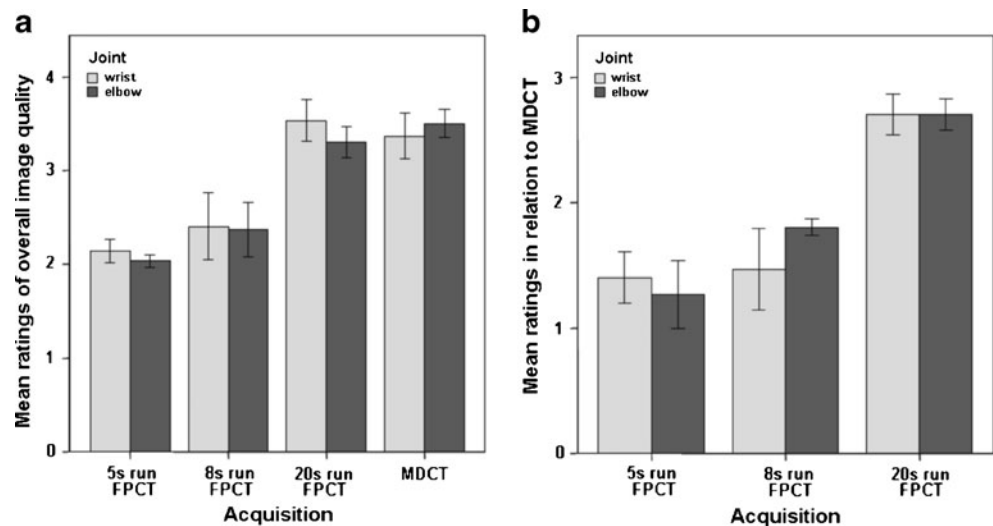
similar image quality, but remarkably exceeds standard MDCT in terms of contrast-to-noise ratio.

Increasing iodine concentrations in the advanced biological joint phantoms led to increasing CT numbers and contrast material noise with a positive correlation for all acquisition protocols and both modalities. For both FPCT and MDCT default settings of tube voltage from the vendors were used (70 kV and 120 kV respectively). Attenuation increased more markedly in FPCT than in MDCT with increasing iodine concentrations. This can be explained by the known attenuation characteristics of iodine at lower tube potentials, thereby nearing the k-edge of iodine [29, 30]. These findings are in accordance with a recent study proving the feasibility of FPCT arthrography in pig ankle joints and investigating the effects of different iodine concentrations on contrast attenuation and CNR using nonbiological joint imitations [24].

Further corroborating published data, a strong correlation between radiation dose and increasing iodine concentrations was also observed for all three FPCT protocols in this study. This effect is explained by the automated exposure control of the FPCT unit, where opaque materials (e.g., high iodine concentrations) cause increased attenuation of X-rays and consecutively a compensatory increase in radiation dose. A similar algorithm was also used for MDCT (i.e., attenuation-based tube current modulation)—however, radiation doses did not vary significantly in relation to increasing iodine concentrations. This indicates that the attenuation-based tube current modulation algorithm of MDCT is less susceptible to changes in attenuation than that from C-arm FPCT.

Flat-panel CT and MDCT also differ with regard to X-ray beam geometry (cone-beam vs fan-beam) and acquisition parameters impacting on radiation dose [9, 10]. In contrast to FPCT, radiation dose in MDCT is not only influenced by tube voltage and tube current, but additionally by the pitch, i.e., the speed at which the object is translated through the scan plane in relation to collimation. While z-coverage in MDCT is theoretically unlimited, it is fixed in FPCT owing to a fixed table position and z-length of the FP detector, which may only be collimated to smaller fields-of-view. However, since the size of the FP detector in our unit is similar to most commercially available angiographic FP units and measures 30×38 cm, z-coverage does not pose a problem for CT arthrography. Tube current is automatically adapted by the FPCT gantry's automatic exposure control and may vary between different projections of a single 200° rotation. The radiation dose of FPCT mainly depends on the predefined angulation increments in the different acquisition protocols of a standard flexible C-arm rotation. This fact is reflected by the increasing scan durations of the three different FPCT acquisition protocols that were used in this study and hence, in increasing dose–area products.

As a result of differences in acquisition technique and radiation dose, tissue contrast and image artifacts differ between acquisition protocols and differences in optimal concentrations of iodinated contrast media can be expected when attempting to compare FPCT with MDCT arthrography with advanced biological joint phantoms. Our results of qualitative data analysis from these phantoms show that for MDCT arthrography a range of different concentrations of iodinated contrast material resulted in high overall image and anatomical depiction quality. In addition, CNRs for different tissue types in advanced joint phantoms increased with increasing iodine concentrations. This may explain why higher iodine concentrations are usually preferred in daily routine practice. The optimal range of iodine concentration for FPCT arthrography was likely to be smaller due to the lower tube voltage and a stronger dependence of image artifacts on high attenuating structures, e.g., iodine or calcium. Furthermore, CNR values of cartilage and soft tissue in animal joint phantoms also peaked at the same iodine concentration. Our experiments in joint phantoms

using biological tissue from pig knees indicated an optimal iodine concentration of 45 mg/ml. This is slightly lower than the iodine concentration found to work best in artificial non-biological joint phantoms (75 mg/ml) in a recent study [24]. An explanation for this difference might be that in that latter study water bottles were used as phantoms to imitate human joints and contrast media containing tubes as phantoms to imitate joint space. In our study, we went a step further and determined the optimal iodine concentration in advanced joint phantoms composed of real biological tissue (cartilage, bone, and soft tissue) in a first step and evaluated its application in human cadaveric joints in a second step.

In FPCT acquisitions of this study, CNR for bone tissue was highest at zero iodine content and decreased with increasing iodine concentration. This might be explained by decreasing differences in CT numbers between bone tissue and contrast material. Interestingly, CNR of bone showed a marked decrease at an iodine concentration of 15 mg/ml, an effect that might be explained by the high image noise in relation to the low differences in CT numbers between bone and contrast material.

Based on the results from quantitative and qualitative image data analysis of the advanced joint phantoms, we performed all subsequent human cadaveric joint arthrographies at an iodine concentration of 45 mg/ml. This decision was based on a trade-off between an adequately high CNR for different joint tissues and low iodine concentration on the one hand, and low radiation dose levels with minimal contrast-induced beam hardening artifacts and image noise on the other hand.

In human cadaveric joint FPCT arthrographies, CNRs of all tissue types were equal to or higher than for MDCT. The best overall image quality was seen in the 20-s FPCT runs for both joints and image ratings of direct comparisons between modalities showed superior depiction of anatomical structures for the 20-s FPCT runs compared with MDCT. Although radiation dose was considerably reduced in 8-s compared with 20-s runs, anatomical depiction remained only a little inferior to MDCT. Even the low radiation dose 5-s FPCT runs provided acceptable depictability.

First, we must acknowledge the inherent limitations of an ex vivo study design and the lack of studies in humans, which may be associated with different image quality and CNR compared with cadavers. Second, joint phantoms were spherical in geometry with a diameter of 8 cm and biological tissue was taken from cadaveric knees of pigs. Human wrists or elbows, however, may have slightly smaller joint volumes compared with our cadaveric phantoms. It is therefore possible, that the optimal iodine concentration derived from our joint phantoms could be different to the optimum in human cadaveric joints. Optimal determination of the iodine concentration should be repeated in the cadaveric wrists. Nevertheless, our phantoms allowed a good reproducibility of quantitative and qualitative data for both CT modalities. Third, we compared different FPCT with a standard 120 kV MDCT protocol. Tube voltage and current may also be adjusted in MDCT and different MDCT protocols might be used. This may potentially lead to increased CNRs of tissue components in MDCT.

Conclusion

The optimal iodine concentration for C-arm FPCT arthrography in this study is 45 mg/ml, leading to superior CNR and image quality for an optimal FPCT protocol compared with standard MDCT arthrography in human cadaveric joints. Future studies should evaluate C-arm FPCT arthrography in vivo and assess the potential of this modality to transduce its superior spatial resolution into an improved depiction of small cartilage defects.

Conflict of interest The authors declare that they have no conflicts of interest.

References

1. Roemer FW, Crema MD, Trattnig S, Guermazi A. Advances in imaging of osteoarthritis and cartilage. Radiology. 2011;260 (2):332–54.
2. De Filippo M, Bertellini A, Pogliacomi F, Sverzellati N, Corradi D, Garlaschi G, et al. Multidetector computed tomography arthrography of the knee: diagnostic accuracy and indications. Eur J Radiol. 2009;70(2):342–51.
3. De Filippo M, Pogliacomi F, Bertellini A, Araoz PA, Averna R, Sverzellati N, et al. MDCT arthrography of the wrist: diagnostic accuracy and indications. Eur J Radiol. 2010;74(1):221–5.
4. Cochet H, Pele E, Amoretti N, Brunot S, Lafenetre O, Hauger O. Anterolateral ankle impingement: diagnostic performance of MDCT arthrography and sonography. AJR Am J Roentgenol. 2010;194(6):1575–80.
5. Fischer W, Bohndorf K, Kreitner KF, Schmitt R, Wortler K, Zentner J. Indications for CT and MR arthrography–recommendations of the musculoskeletal workgroup of the DRG. Rofo. 2009;181(5):441–6.
6. El-Khoury GY, Alliman KJ, Lundberg HJ, Rudert MJ, Brown TD, Saltzman CL. Cartilage thickness in cadaveric ankles: measurement with double-contrast multi-detector row CT arthrography versus MR imaging. Radiology. 2004;233(3):768–73.
7. Prokop M. General principles of MDCT. Eur J Radiol. 2003;45 Suppl 1:S4–10.
8. De Filippo M, Bertellini A, Sverzellati N, Pogliacomi F, Costantino C, Vitale M, et al. Multidetector computed tomography arthrography of the shoulder: diagnostic accuracy and indications. Acta Radiol. 2008;49(5):540–9.
9. Kyriakou Y, Struffert T, Dorfler A, Kalender WA. Basic principles of flat detector computed tomography (FD-CT). Radiologe. 2009;49(9):811–9.
10. Kalender WA, Kyriakou Y. Flat-detector computed tomography (FD-CT). Eur Radiol. 2007;17(11):2767–79.
11. De Cock J, Mermuys K, Goubau J, Van Petegem S, Houthoofd B, Casselman JW. Cone-beam computed tomography: a new low dose, high resolution imaging technique of the wrist, presentation of three cases with technique. Skeletal Radiol. 2012;41(1):93–6.

12. Ramdhian-Wihlm R, Le Minor JM, Schmittbuhl M, Jeantroux J, Mahon PM, Veillon F, et al. Cone-beam computed tomography arthrography: an innovative modality for the evaluation of wrist ligament and cartilage injuries. Skeletal Radiol. 2012;41 (8):963–9.

13. Wang G, Crawford CR, Kalender WA. Multirow detector and cone-beam spiral/helical CT. IEEE Trans Med Imaging. 2000;19 (9):817–21.

14. Schulze R, Heil U, Gross D, Bruellmann DD, Dranischnikow E, Schwanecke U, et al. Artefacts in CBCT: a review. Dentomaxillo-fac Radiol. 2011;40(5):265–73.

15. Jelinek J, Overton TR. Simulation of CT reconstruction artifacts associated with multiple-rotation fan-beam data collection. Comput Radiol. 1986;10(1):23–36.

16. Schindera ST, Diedrichsen L, Muller HC, Rusch O, Marin D, Schmidt B, et al. Iterative reconstruction algorithm for abdominal multidetector CT at different tube voltages: assessment of diagnostic accuracy, image quality, and radiation dose in a phantom study. Radiology. 2011;260(2):454–62.

17. Struffert T, Deuerling-Zheng Y, Kloska S, Engelhorn T, Strother CM, Kalender WA, et al. Flat detector CT in the evaluation of brain parenchyma, intracranial vasculature, and cerebral blood volume: a pilot study in patients with acute symptoms of cerebral ischemia. AJNR Am J Neuroradiol. 2010;31(8):1462–9.

18. Penzkofer T, Isfort P, Bruners P, Wiemann C, Kyriakou Y, Kalender WA, et al. Robot arm based flat panel CT-guided electromagnetic tracked spine interventions: phantom and animal model experiments. Eur Radiol. 2010;20(11):2656–62.

19. Struffert T, Richter G, Engelhorn T, Doelken M, Goelitz P, Kalender WA, et al. Visualisation of intracerebral haemorrhage with flat-detector CT compared to multislice CT: results in 44 cases. Eur Radiol. 2009;19(3):619–25.

20. Suzuki S, Yamaguchi I, Kidouchi T, Yamamoto A, Masumoto T, Ozaki Y. Evaluation of effective dose during abdominal three-dimensional imaging for three flat-panel-detector angiography systems. Cardiovasc Intervent Radiol. 2011;34(2):376–82.

21. Phan CM, Macklin EA, Bredella MA, Dadrich M, Flechsig P, Yoo AJ, et al. Trabecular structure analysis using C-arm CT: comparison with MDCT and flat-panel volume CT. Skeletal Radiol. 2010;40(8):1065–72.

22. Walsh CJ, Phan CM, Misra M, Bredella MA, Miller KK, Fazeli PK, et al. Women with anorexia nervosa: finite element and trabecular structure analysis by using flat-panel volume CT. Radiology. 2010;257(1):167–74.

23. Bredella MA, Misra M, Miller KK, Madisch I, Sarwar A, Cheung A, et al. Distal radius in adolescent girls with anorexia nervosa: trabecular structure analysis with high-resolution flat-panel volume CT. Radiology. 2008;249(3):938–46.

24. Guggenberger R, Fischer MA, Hodler J, Pfammatter T, Andreisek G. Flat-panel CT arthrography: feasibility study and comparison to multidetector CT arthrography. Invest Radiol. 2012;47(5):312–8.

25. Moser T, Dosch JC, Moussaoui A, Buy X, Gangi A, Dietemann JL. Multidetector CT arthrography of the wrist joint: how to do it. Radiographics. 2008;28(3):787–800. quiz 911.

26. Steinbach LS, Schwartz M. Elbow arthrography. Radiol Clin North Am. 1998;36(4):635–49.

27. Cohen J. Weighted kappa: nominal scale agreement with provision for scaled disagreement or partial credit. Psychol Bull. 1968;70 (4):213–20.

28. Landis JR, Koch GG. The measurement of observer agreement for categorical data. Biometrics. 1977;33(1):159–74.

29. Huda W, Scalzetti EM, Levin G. Technique factors and image quality as functions of patient weight at abdominal CT. Radiology. 2000;217(2):430–5.

30. Nakayama Y, Awai K, Funama Y, Hatemura M, Imuta M, Nakaura T, et al. Abdominal CT with low tube voltage: preliminary observations about radiation dose, contrast enhancement, image quality, and noise. Radiology. 2005;237(3):945–51.